Nano Research

Open Access

Research Article

Dual-color center diamond for concealable physically unclonable functions

Fuhang Jiao[1,§], Junlu Sun[1,§], Chaonan Lin[2] ✉, Ying Xiao[3], Zhenfeng Zhang[1], Yuan Deng[4], Haizhong Guo[1,2], Shunfang Li[1], Lijun Wang[1], Chong-Xin Shan[1] ✉, and Lin Dong[1] ✉

[1] *Henan Key Laboratory of Diamond Optoelectronic Materials and Devices, Key Laboratory of Integrated Circuit, Ministry of Education, School of Physics, Zhengzhou University, Zhengzhou 450001, China*
[2] *Institute of Quantum Materials and Physics, Henan Academy of Sciences, Zhengzhou 450003, China*
[3] *Department of Ophthalmology, Shandong Provincial Hospital Affiliated to Shandong First Medical University, Jinan 250021, China*
[4] *School of Computational Science and Electronics, Hunan Institute of Engineering, Xiangtan 411104, China*
§ *Fuhang Jiao and Junlu Sun contributed equally to this work.*

Cite this article: *Nano Research*, **2025**, *18*, 94907905. https://doi.org/10.26599/NR.2025.94907905

ABSTRACT: Physical unclonable functions (PUFs) offer a promising defensive measure against the escalating challenges posed by the increasingly rampant counterfeit products. Conventional PUF materials with a singular physical property encounter limitations in encoding flexibility and capacity. Here, we propose a dual-color center diamond-based PUF (D-PUF) ink that exploits four diverse optical characteristics of dual-color center in diamond to design a concealable multi-level cryptographic authentication protocol. Through simple writing, stamping, or spraying, intricate covert random patterns can be directly generated on the objects, which are imperceptible under visible light. When challenged by a 532 nm laser, the D-PUF exhibits four distinct optical responses, including Raman, zero phonon line (ZPL) of germanium vacancies (GeV), ZPL of silicon vacancies (SiV), and the intensity ratios of these ZPLs. These responses were harvested simultaneously to construct the four-level separate encodable matrices. Furthermore, M-ary encoding algorithms were implemented to encrypt PUFs with flexibility. The resulting multi-level PUF system attains notable uniqueness, repeatability, extensive encoding capacity (> 10^{48164}/(100 pixels)^2), and ultra-high information entropy (6 bits/pixel). This study inspires designing new generations of multi-level PUFs with enhanced coding flexibility and holds significant promise for applications in print security.

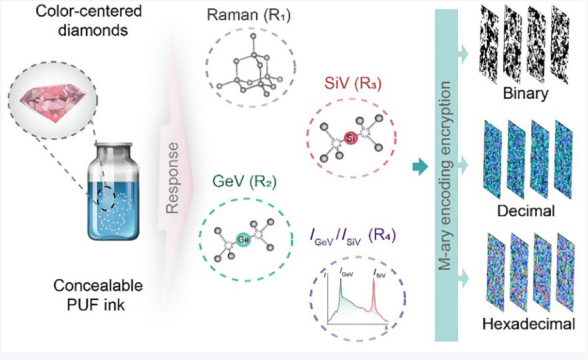

KEYWORDS: physical unclonable function, dual-color center diamond, silicon vacancy, germanium vacancy, anti-counterfeit

1 Introduction

Printing forgeries, such as counterfeit currency, forged seals, and imitated artworks, remain a persistent global challenge. Its repercussions extend beyond economic destabilization, impacting the public interest, violating intellectual property rights, and posing threats to human security [1, 2]. Modern anti-counterfeiting technologies, such as watermarking [3], holographic color printing [4], fluorescent security inks [5, 6], phosphorescent inks [7], and magnetic inks [8], have emerged as effective defenses against this growing menace. Nevertheless, the ever-evolving landscape of counterfeiting techniques renders deterministic encoding mechanisms increasingly susceptible to cloning attacks. To address these security vulnerabilities, physical unclonable functions (PUFs), which leverage inherently random physical features to generate unique and unpredictable identifiers, have emerged as a promising alternative solution [9–11]. Indeed, PUF manufacturing processes are stochastic and uncontrollable, making replication extremely challenging. Various PUFs based on stochastic physical features, such as Raman [12], photoluminescence [13, 14], polarization [15], light diffraction [16, 17], fractal-network [18], wrinkles [19, 20], and symmetry breaking [21], have been designed and developed for use in diverse anti-counterfeiting applications.

Received: June 4, 2025; **Revised:** August 2, 2025
Accepted: August 7, 2025

✉Address correspondence to Chaonan Lin, Lin2024@hnas.ac.cn; Chong-Xin Shan, cxshan@zzu.edu.cn; Lin Dong, ldong@zzu.edu.cn

Despite the high security offered by PUFs, with the explosion of machine learning, the demand for PUF encoding capability is increasing to an extent that single-mode challenge responses struggle to cope [22, 23]. Multimode PUFs exponentially raise the ceiling of PUF encoding capacity by integrating different anti-counterfeiting structures or response modes and harnessing the synergies between them [24, 25]. Furthermore, the combination of multiple anti-counterfeiting means, such as integrating PUFs with quick response (QR) codes or employing PUFs based on different random physical characteristics, can simultaneously improve security and reliability [26–28]. However, potential crosstalk between signals from different layers may impact coding independence, and the stereotypical encoding concept may limit the cryptographic flexibility of PUF.

Diamond, with its exceptional physicochemical stability, biocompatibility, outstanding optical properties, and abundant luminescent point defects, presents significant potential for applications in various fields, such as biosensing [29] and quantum probing [30], etc. Notably, the diverse optical structures of diamond (e.g., Raman scattering, color center luminescence, etc.) endow it with abundant spectral features, making it an ideal seed material for constructing PUFs [31, 32]. Particularly, the diamond color center, whose formation involves complex physicochemical processes, features intrinsic randomness in the concentration and spatial distribution of atomic defects in the crystal lattice, which renders the diamond color center-based PUF system irreproducible and impervious to cloning through micro-nano machining, thus significantly enhancing the safety of PUFs. Recent works have indicated that the multiple optical degrees of freedom (DoF) (e.g., spatial distribution, phase, polarization, etc.) of diamond nitrogen-vacancy (NV) color centers can provide unique optical responses, thus enabling multilevel PUF encoding [33, 34]. Nevertheless, this approach relies on a complex optical modulation system and sophisticated optical components, resulting in higher usage cost that limits its practical application. Additionally, silicon vacancy (SiV) and germanium vacancy (GeV) color centers in diamond exhibit narrow-band emission properties, which have been employed to develop traceable optical PUF systems [35, 36]. However, the single-emitter mode limits the dimensional expansion of optical encoding. While the multi-emitter integration strategy promises to achieve multidimensional PUF encoding, the scheme requires the signals to remain independent from each other to avoid crosstalk. Interstitial atom-doped diamond color centers, such as group IV defects, exhibit mutually non-overlapping narrow-band emission, allowing distinguishable responses from various emitters [37, 38]. Thus, multi-color center diamond random seeds coupled with M-ary encoding technology can fulfill the requirements for manufacturing multi-level PUFs with flexible and scalable encoding.

In this work, we present a multi-level PUF system based on the distinct optical characteristics of micron-sized dual-color center diamond. These diamonds, emitting narrowband light, were incorporated with invisible fluorescent inks yielded by 7-amino-4-methylcoumarin (AMC) to create PUF inks, which allow the generation of intricate random patterns on objects through simple writing, sealing, or spraying processes. The patterns, drawn with invisible fluorescent ink, were utilized to store anti-counterfeiting information and serve as positioning markers for the PUFs. Under the excitation of a 532 nm laser, four distinct responses of the diamond, i.e., Raman (R_1), zero phonon line (ZPL) of GeV (R_2), ZPL of SiV (R_3), and I_{GeV}/I_{SiV} (R_4), were collected simultaneously to create four independent codable matrices. To enhance flexibility in encoding, multi-level encryption of the PUF was performed using customized M-ary encoding procedures and corresponding authentication algorithms. Each PUF operates independently, ensuring accurate authentication. This multi-level PUF system achieves a remarkable encoding capacity, holding significant promise for applications in print security. This strategy combines the unique properties of dual-color center diamonds with advanced encoding techniques, paving the way for enhanced anti-counterfeiting measures and robust security applications.

2 Results and discussion

To enhance the security of high-value printed products like banknotes and cheques, there is a growing need for reliable security measures, a demand for authenticity and security that PUF inks aim to fulfill. As illustrated in Fig. 1(a), our PUF ink application for print safety delivers dual encryption modes to boost security. At macro scale, security marks such as QR codes or barcodes generated by fluorescent inks offer conventional fingerprint information for general verification. At micro scale, random optical distribution patterns generated by dual-color center diamonds contribute multiple cryptographic details for highly reliable authentication processes. Importantly, each signal is collected contactless in light form, preventing physical damage to the products during the authentication process.

The design principle and encoding strategy of the PUF ink based on dual-color center diamonds were illustrated in Fig. 1(b). The invisibility of the fluorescent ink under visible light enables it to conceal specific pattern information as anti-counterfeiting identifiers. The security information is legible under ultraviolet (UV) excitation, providing finite security. Furthermore, the dual-color center diamonds deliver four distinct response signals, including Raman (R_1), ZPL of GeV (R_2), ZPL of SiV (R_3), and I_{GeV}/I_{SiV} (R_4), which can be read simultaneously under 532 nm excitation, thus facilitating the efficiency of multi-level PUF collection. It is worth mentioning that the specific identifier formed by the fluorescent ink can act as a positioning marker for the D-PUF to ensure the reproducibility of the PUF measurement, a method also recognized by many strategies [14, 39, 40]. The obtained response matrices can be separately encrypted by specific extractors to yield the final cryptographic keys.

The foundation for constructing multi-level PUFs lies in the distinctive physical characteristics exhibited by dual-color center diamonds. Figure 2(a) depicts representative PL spectra of the dual-color center diamonds, which exhibit sharp narrow-band spectral responses at 572, 602, and 738 nm, corresponding to Raman of diamond, ZPL of GeV, and ZPL of SiV, respectively. Both GeV and SiV color centers are formed by an interstitial impurity atom located between two adjacent lattice vacancies (Fig. S1 in the Electronic Supplementary Material (ESM)), featuring inversion symmetry, which results in the fluorescence emission mainly concentrated near the ZPL, manifesting a narrow-band emission characteristic. The high-contrast narrowband emission of dual-color center diamonds allows easy distinction of the three separate spectral responses, enabling simultaneous capture of broadband spectrum for efficient signal acquisition. Furthermore, these three distinct spectral responses exhibited remarkable stability in optical signals under continuous 100 min excitation, shown in Fig. S2 in

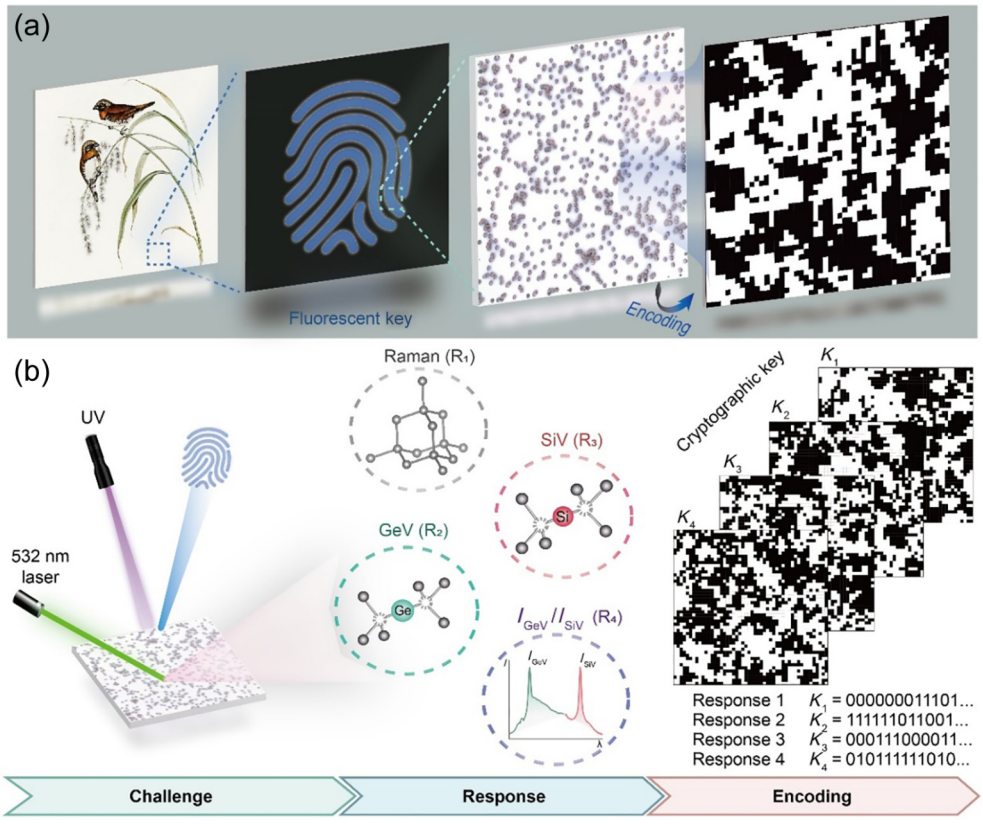

Figure 1 Application scheme based on dual-color center diamond-based PUF ink and the encoding strategy. (a) Illustration description of PUF ink applied to prints. (b) Flowchart of multi-level PUF key production. Four distinct responses from the dual-color center diamond were employed for multimodal encoding.

the ESM, contributing to ensuring the reliable performance of PUF tags over multiple readout cycles. It is worth noting that these diamonds were prepared using the microwave plasma chemical vapor deposition (MPCVD) method, utilizing a germanium-coated substrate and a silicon wafer as doping sources. Unlike the controlled process of high-pressure/high-temperature (HPHT) [41] or ion implantation [42], the silicon-germanium co-doped diamonds prepared through MPCVD exhibit desirable unpredictability and randomness, which is crucial for PUF applications. The randomness of dual-color center diamonds stems from the following points: first, the doping concentration of silicon and germanium atoms in diamond is difficult to precisely control. Even under the same process conditions, the concentrations of SiV and GeV in the diamond prepared each time can be different. Second, the spatial position of silicon and germanium atoms in the diamond lattice is unpredictable. Stochastic doping positions will influence the optical properties of the color centers. Third, there exists randomness in the size, surface morphology, and crystalline quality of diamond, which can affect the properties and distribution of the color centers. Notably, by enriching the precursor substances, the diversity of color center defects in diamond can be effectively expanded to obtain abundant optical response properties.

Scanning electron microscopy (SEM) observation reveals a haphazard size and morphology distribution, with sizes ranging from 1–12 μm (Fig. S3 in the ESM), favoring the chaotic nature of the D-PUFs that makes their replication challenging. It should be mentioned that nanoscale color center diamonds can be employed to significantly improve spatial resolution and integration flexibility, yet technical barriers such as weak fluorescence signals from single particles and complex optical readout setups remain to be resolved. X-ray diffraction (XRD) of the dual-color center diamonds exhibits three distinct peaks with a narrow full width at half-maximum (FWHM), as shown in Fig. S4 in the ESM, indicating excellent crystalline quality of the diamonds [43]. Subsequently, the fluorescence lifetimes of SiV and GeV were determined, as depicted in Fig. 2(b). Under the excitation of a 475 nm picosecond laser, SiV and GeV exhibited lifetimes of 1.18 and 1.59 ns, respectively. Both color centers display a short fluorescence lifetime, which helps to avoid fluorescence interference during rapid PUF acquisition.

To obtain the PUF ink, the dual-color center diamonds were pretreated via a wet chemical treatment (acid mixtures) and then mixed with fluorescent ink of 7-amino-4-methylcoumarin (Fig. S5 in the ESM). Chemical treatment with oxidizing acids allows cleaning of the diamond surface while increasing the positive electron affinity (PEA) and hydrophilicity of the diamond, which are favorable for achieving stable aqueous dispersion [44, 45]. Fourier transform infrared (FTIR) spectra in Fig. 2(c) reveal the C–O stretching mode of the hydroxyl group at around 1089 cm^{-1}, C=O stretching at around 1630 cm^{-1}, and C–OH stretching at around 3437 cm^{-1}, respectively, indicating that the treated diamonds possess abundant hydrophilic groups. Note that the selection of fluorescent ink is critical to avoid interference during the PUF acquisition process. Figure S6 in the ESM shows the absorption and UV-excited fluorescence spectra of the fluorescent inks used, with no significant absorption at 532 nm and emission concentrated mainly from 400 to 530 nm. Obviously, the fluorescent ink differs significantly from diamond in spectrum, thus the adoption of fluorescent ink poses no detrimental interference to the detection and separation of diamond spectral signals.

PUF ink offers versatile applications for generating randomized

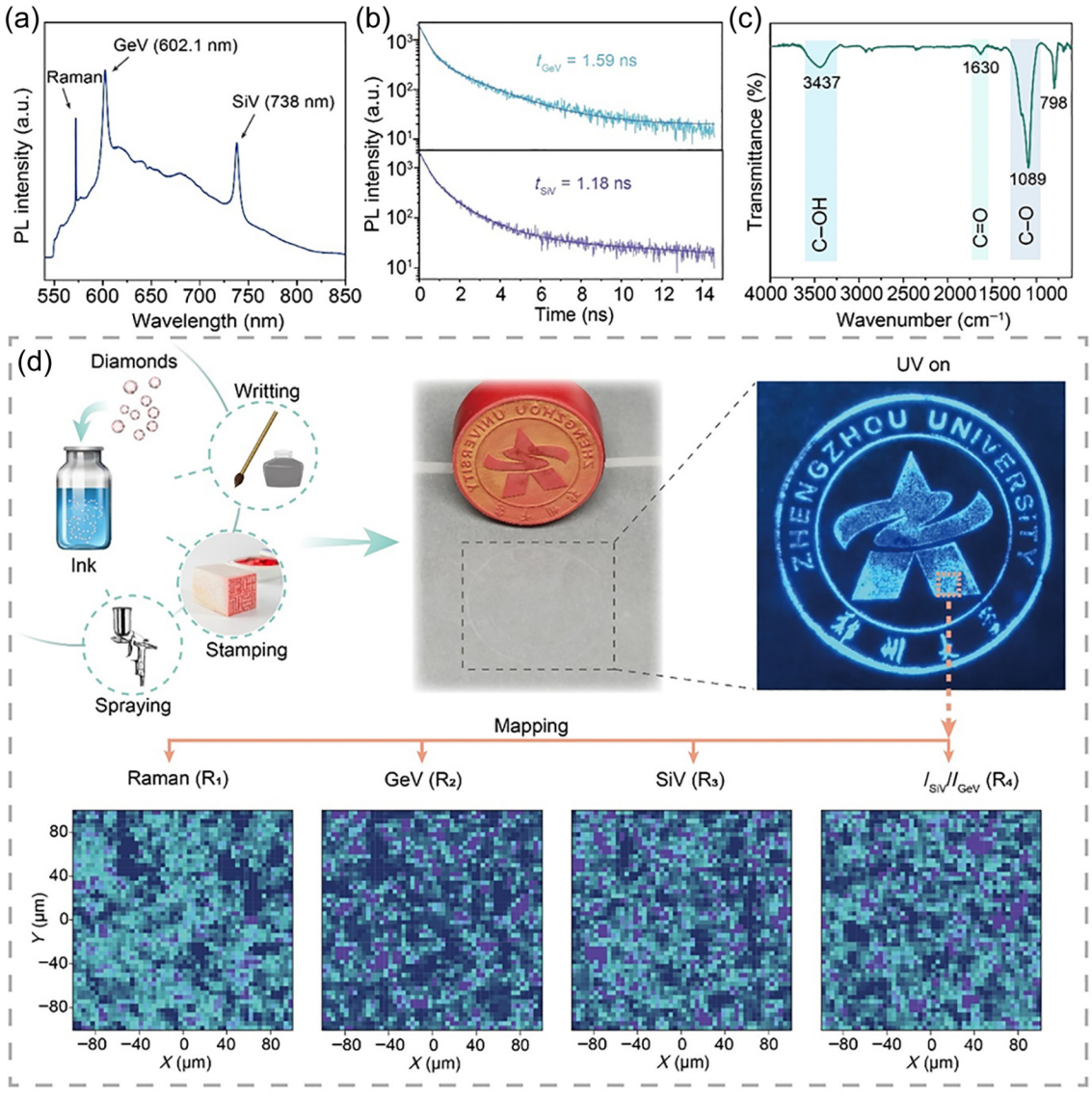

Figure 2 Preparation and characterization of dual-color center diamond-based PUF ink. (a) PL spectrum of dual-color center diamonds excited by a 532 nm laser. (b) PL decay curves collected at the emission peaks of 602 and 738 nm for dual-color center diamond. (c) FTIR spectrum of dual-color center diamonds. (d) Description of the fabrication and application process of dual-color center diamond-based PUF inks.

patterns on object surfaces, including but not limited to writing, stamping, or spraying, which makes them highly adaptable for a broad spectrum of anti-counterfeiting uses, spanning electronic skin [46], pharmaceuticals [47], and beyond. As an exemplary demonstration, we printed a logo pattern on non-fluorescent paper using a seal (Fig. 2(d)). Under visible light, traces of the stamp are barely visible yet become legible under UV excitation, conferring the PUFs with hidden anti-counterfeiting capability. Stochastic patterns driven by dual-color center diamonds for D-PUFs are manifested on smaller scales, as demonstrated in Fig. S7 in the ESM. To execute the D-PUFs, an area of 200 μm × 200 μm was selected for PL mapping at the site of fluorescence, and four different response matrices can be obtained after collecting and segmenting the PL at each point. Among these, the first three levels of responses are predicated on the characteristic Raman, GeV, and SiV responses, respectively, allowing direct acquisition of the corresponding spectral information for subsequent encoding. Whereas, the fourth level response was derived from the ratio of the PL intensities of GeV and SiV. Given the stochastic nature of both GeV and SiV responses, the fourth-level response is likewise random and independent. In practical implementation, the multi-level anti-counterfeiting modes of D-PUF can be utilized individually or jointly, which is conducive to improving the reliability and practicality of PUF. Notably, the cost of a single PUF tag was estimated to be approximately \$0.0000012 (Table S1 in the ESM), making it highly competitive for practical applications.

Figure 3(a) presents four mappings based on different responses obtained from the same PUF and their corresponding binary coding matrices with a resolution of 50 × 50 pixels, demonstrating significant discrepancies. In practice, PUFs can be encoded into matrices with different pixel resolutions (Fig. S8 in the ESM). However, selecting the optimal resolution requires balancing the physical positioning accuracy of diamond microparticles and information utilization efficiency. We isolated and extracted 80 distinct raw data matrices from 20 different D-PUFs and transformed them into binary matrices as shown in Figs. S9–S12 in

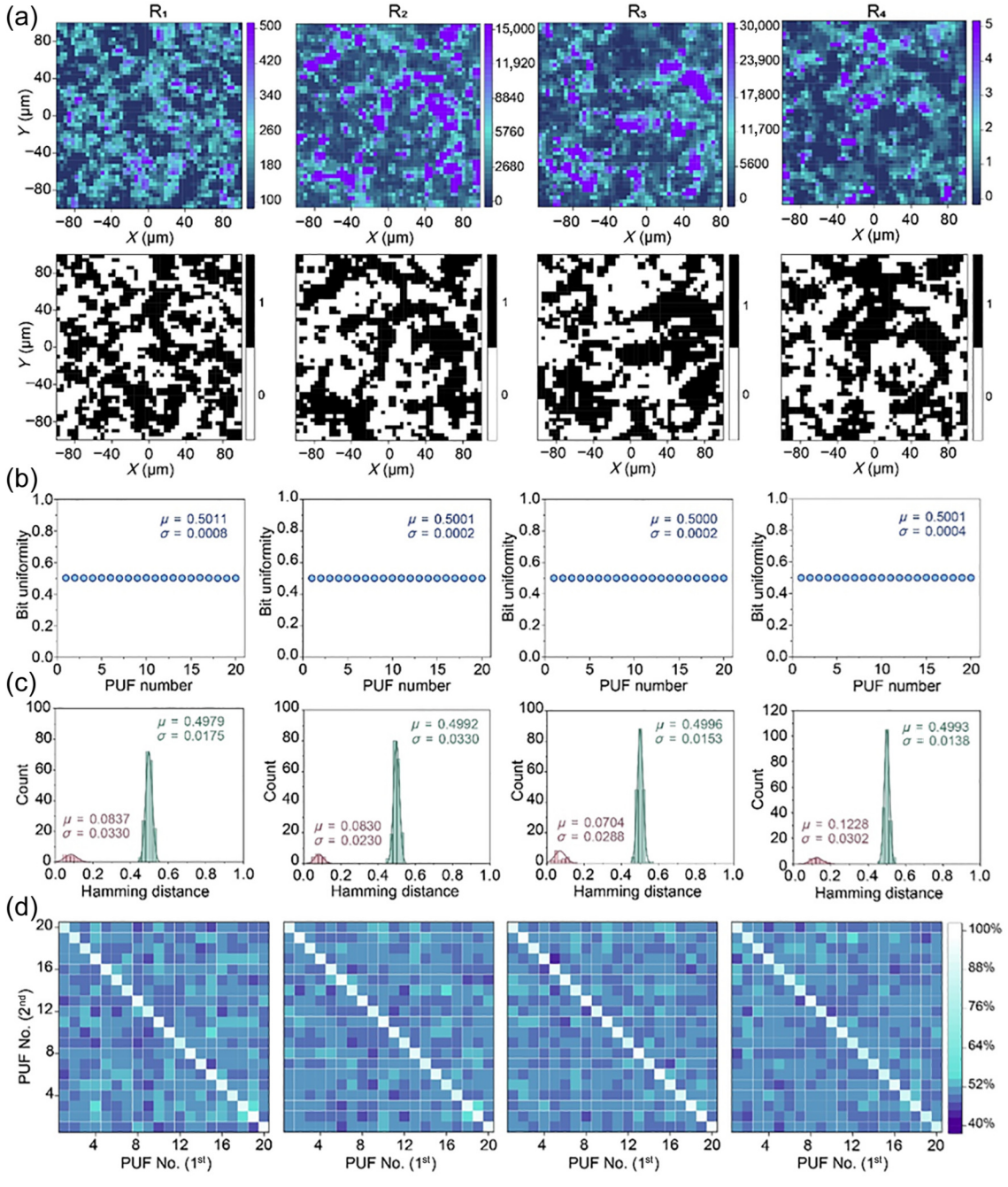

Figure 3 Readout and authentication of dual-color center diamond-based PUF ink with binary coding. (a) PL mapping images of the four different responses from the PUF ink and the corresponding binary coding matrices with a resolution of 50 × 50 pixels. (b) Bit uniformity calculated from four different responses for each of the 20 distinct PUFs. (c) Statistical distribution of inter-device HD and intra-HDs for four different responses derived from each of 20 different PUFs. The inter-HDs of the four responses are 0.4979, 0.4992, 0.4996, and 0.4993, respectively. The intra-HDs of the four responses are 0.0837, 0.0830, 0.0704, and 0.1228, respectively. (d) Pixel-by-pixel pairwise similarity comparisons were performed on the first and second measurements of the four responses from 20 different PUFs, with similarity indices indicated by color bars.

the ESM. Furthermore, the benchmark performance of PUF binary coding was systematically evaluated in terms of bit uniformity, uniqueness, and reproducibility. Bit uniformity was employed to estimate the probability of the occurrence of the digits 0 and 1 in the PUF binary coding matrix, converging to the ideal value of 0.5, where the binary sequence is most chaotic and difficult to predict. For each of the four levels of D-PUFs, the median was introduced as the threshold for extracting the bit sequences, with all bit uniformities converging to 0.5 (Fig. 3(b)). To evaluate the uniqueness and reproducibility of the D-PUFs, Hamming distance (HD) was introduced to analyze the number of mismatching bits between bit sequences extracted by PUFs. The bit sequences extracted from different PUFs were computed as inter-HD to assess the uniqueness, while those obtained from multiple acquisitions of the same PUF were calculated as intra-HD to quantify reproducibility. For inter-HD, 190 ($^{20}C_2$) pairs of challenge-response pairs (CRPs) were computed for each response of D-PUF and plotted as histograms, as shown in Fig. 3(c). The mean value of

inter-HD calculated based on the four different responses of the D-PUF is 0.4990, and the standard deviation value is 0.0199, confirming the uniqueness and randomness of each level of PUF. Furthermore, all response-based encoding keys successfully passed NIST randomness tests, demonstrating exceptionally high randomness quality (Tables S2–S5 in the ESM). Moreover, the estimated intra-HD yields a mean value of 0.0899 with a standard deviation of 0.0287, indicating that the PUF possesses good repeatability. Notably, by improving the stability of the detection equipment or increasing the size of the PUF tag, further reductions of the mean intra-HD and the bit error rate are anticipated. For practical implementation, we recommend performing a positional calibration routine prior to each verification to effectively mitigate measurement errors induced by optical angle variations and other environmental factors. Furthermore, implementing specialized encapsulation patterns for the tags may significantly improve PUF system stability in complex operational environments, offering a viable optimization approach for real-world deployment scenarios.

To further investigate the accuracy of the PUF authentication system, the false negative rate was assessed using inter-HD and intra-HD distributions. The false negative rate for all levels of binary coding of the D-PUFs is less than 10^{-13} (Fig. S13 in the ESM), indicating an infinitesimal probability of PUF authentication errors. The uniqueness and reproducibility of the D-PUFs were reaffirmed by analyzing the similarity of 20 different PUFs in pairwise comparisons. As shown in Fig. 3(d), the similarity indices of the non-diagonal regions are all below 50%, suggesting that the PUFs are mostly mutually dissimilar and unique. In contrast, the similarity of the diagonal regions exceeds 85%, indicating that the PUFs are reproducible.

Subsequently, to validate that the PUFs based on different responses are independent of each other, 40 coding matrices were extracted from 10 D-PUFs to compute the HDs (Fig. S14 in the ESM). It is evident that the HDs between twice measurements of the same PUF tend to be 0, while the HDs between different PUFs converge to 0.5, demonstrating the independence and reproducibility of the PUFs based on different responses. Notably, this independence characteristic holds true even when considering the optical physical positions of diamonds (Fig. S15 in the ESM). Furthermore, these multi-level D-PUFs implement independent unclonable patterns at various levels, thereby effectively increasing the complexity and encoding capacity of the PUFs.

Owing to the enormous randomness and diversity of responses at each level of the D-PUF, we augmented multiple thresholds to the encoding process to achieve a more intricate and adaptable high-level PUF encryption (e.g., decimal and hexadecimal). Figure 4(a) presents the decimal coding matrices for the four-level response of the D-PUF, showing a chaotic and complex distribution. Since HD generally describes the number of non-zero values of a string that is not amenable to M-ary encoding, we here assess the feasibility of decimal encoding using the cross-correlation function. This function elucidates the degree of linear correlation between codes, with correlation coefficients (CC) ranging from −1 to 1, converging to 0 signifies no correlation at all, while deviation towards either end indicates varying degrees of correlation. Cross-correlation analysis was employed to authenticate response matrices from 20 D-PUFs across various levels, revealing significant variations between diagonal and non-diagonal regions (Fig. 4(b)). Statistical analysis of the correlation coefficients, as depicted in Fig. 4(e), reveals correlation coefficients ranging from −0.15 to 0.15, converging to 0, while those within the same PUFs converge to 1, indicating the efficacy of decimal encoded PUFs for accurate authentication.

Similarly, the feasibility of hexadecimal encoding of the D-PUFs was also investigated. The hexadecimal coding matrices of the D-PUFs exhibit a more heterogeneous and intricate code element distribution (Fig. 4(c)), with discernible variation between diagonal and non-diagonal regions in pairwise comparison maps (Fig. 4(d)). Furthermore, the correlations between hexadecimal encoded PUFs can be accurately discerned from the statistical distribution of the correlation coefficients in Fig. 4(f), similar to decimal coding.

Apparently, adjusting the number of thresholds to change the length of encoding code elements facilitates M-ary coding of PUFs, allowing for accurate authentication via the cross-correlation function, which enhances the adaptability, security, and reliability of the PUF encoding greatly. Moreover, as the length of the code element increases, the information entropy of a single pixel in the D-PUF significantly rises, with hexadecimal coding approaching 6 bits per pixel. The extraordinarily high information entropy means that this multi-level PUF encoding system possesses an extremely high degree of complexity and chaos, making it unpredictable, thereby favoring the security of the PUF. Besides, the multi-level PUF coding system's tremendous coding capacity, estimated to exceed 10^{48164}/(100 pixel)^2, accommodates the requirements of most authentication systems. This capacity demonstrates superior competitiveness compared to currently reported PUF systems, as shown in Table S6 in the ESM. Furthermore, if necessary, the coding capacity can be exponentially increased by expanding the capture size of the PUF or increasing the length of the encoding code elements.

The reliability of PUF tags is of paramount importance for practical deployment, as it directly determines the system's authentication accuracy and long-term stability. Figure S16 in the ESM demonstrates the PUF tag's excellent stability across repeated measurements, confirming its exceptional reliability for practical applications. We further evaluated the stability of D-PUFs in various environments to validate its true reliability. As shown in Fig. S17 in the ESM, when the D-PUFs tag was heated up to 100 °C, the intra-HD of its four responses were 0.0928, 0.0816, 0.0968, and 0.1128, respectively, which demonstrated excellent thermal stability. Figure S18 in the ESM presents the stability of D-PUFs exposed to environmental conditions for different time. Thanks to the excellent physicochemical stability of the dual-color center diamonds, the D-PUFs maintained excellent verifiability after exposure to ambient conditions for 60 days. Furthermore, the D-PUFs were subjected to different humidity environments for 24 h to examine their humidity stability. D-PUFs exhibited excellent reliability under relative humidity of less than 79% (Fig. S19 in the ESM). However, the validation error in higher humidity environments turns larger, which is mainly attributed to the excellent hydrophilicity of the D-PUF ink. Therefore, it is recommended that D-PUF be utilized in relatively low-humidity environments, which is also in accordance with the regular preservation standards for print products.

Figure 5(a) illustrates the schematic of the complete authentication system based on D-PUF. Initially, the manufacturers batch produce anti-counterfeit labels using PUF ink and record the PL signal mappings of the produced labels. These mappings are segmented into four-level PUFs according to the characteristic responses, and multiple M-ary encryption keys are derived and stored in a cloud database for subsequent authentication. The above registration process of the D-PUFs is completed by the

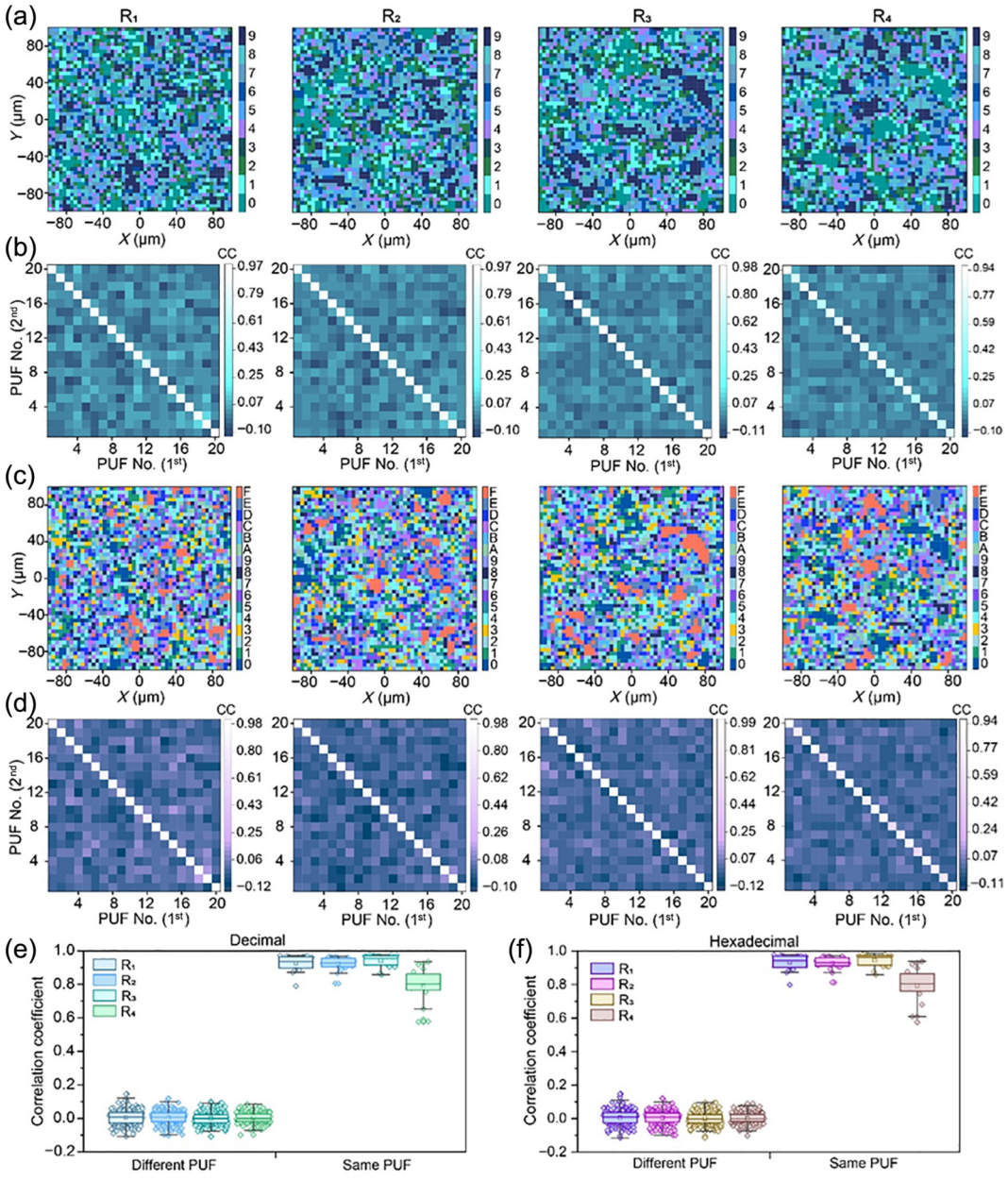

Figure 4 Authentication of dual-color center D-PUF ink with M-ary encoding. (a) The decimal encoding matrices of the four different responses from the PUF ink and with a resolution of 50 × 50 pixels. (b) Pairwise comparisons as a cross-correlation function on the decimal encoding of the first and second measurements of the four responses from 20 different PUFs, with the CC indicated by the color bars. (c) The hexadecimal encoding matrices of the four different responses from the PUF ink and with a resolution of 50 × 50 pixels, indicating low false positive rates. (d) Pairwise comparisons as a cross-correlation function on the hexadecimal encoding of the first and second measurements of the four responses from 20 different PUFs, with the CC indicated by the color bars. (e) Box plot of the cross-correlation function of D-PUFs with decimal encoding. (f) Box plot of the cross-correlation function of D-PUFs with hexadecimal encoding.

manufacturers. Registered PUF labels accompany products through the supply chain, undergoing multiple authentications before reaching the end users. As the labels circulate, authentication occurs at each stage to ensure product traceability. The verifier scans and digitizes the unknown PUF label and uploads the digitized key to the cloud database for authentication. Then, the unknown digitized key is compared with the key in the database by calculating HDs or correlation coefficients: If higher than the pre-set threshold, the verification passes; otherwise, the verification fails. Given the variability in scanning environments, the authentication threshold can be adjusted appropriately to accommodate minor errors according to the actual usage. Additionally, after the authentication failure, the validator is prompted to collect better raw data for further validation.

The process of encryption and decoding of PUF ink applied to a cheque is exemplified in Fig. 5(b). First, a specific QR code was stamped on the cheque using PUF ink, which is barely detectable in visible light. Under UV excitation, concealed identifiers can be detected, and the stored information can be read. After the location was determined by the fluorescent identifier, the D-PUF was captured and encoded into M-ary matrices for subsequent comparison with the database for authentication. Overall, the security of the cheque was significantly enhanced by employing the multi-level D-PUFs to encrypt the cheque information. Moreover,

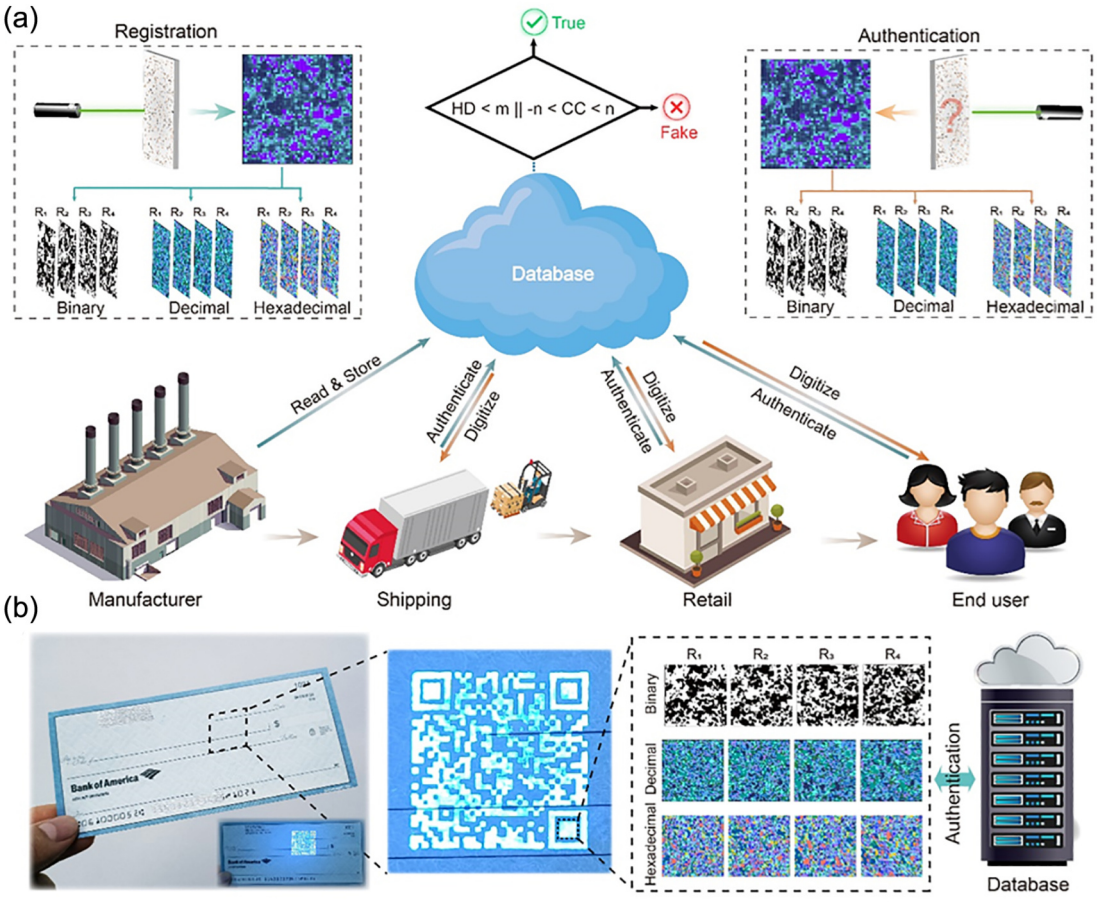

Figure 5 Encryption and authentication flow of the multi-level D-PUFs. (a) Conceptual illustration of the D-PUFs usage process. PUFs were read and uploaded to the database to complete system registration prior to circulation; the end user could decode the circulating PUF by capturing and uploading the PL mapping data to the database. (b) Illustration of the encryption and decoding process of D-PUF on a cheque.

our authentication protocol has been successfully ported to a mobile platform, demonstrating real-time PUF tag verification capabilities (Video S1 in the ESM), though the current implementation remains at a proof-of-concept stage that would benefit from specialized optimization in software engineering and user interface design.

3 Conclusion

In summary, we have presented a concealable PUF ink based on dual-color center diamonds. The inherent optical responses of these diamonds yield four distinct optical patterns for creating multi-level PUFs. The PUF patterns, unique and random, can be utilized individually or in combination to enable robust and adaptable security authentication modes. Meanwhile, the D-PUF architecture engenders independent unclonable patterns across various levels, which can effectively increase the complexity and encoding capacity of PUFs. Additionally, the implementation of M-ary coding facilitated by adjusting thresholds, coupled with accurate authentication via the cross-correlation function, significantly improves the encoding flexibility of the PUF and is anticipated to be a pervasive strategy. The constructed multi-level PUF system demonstrates desirable uniqueness, repeatability, and competitiveness in key parameters, including coding capacity, information entropy, and encoding flexibility. Moreover, the inherent invisibility of the PUF ink under natural light effectively enhances the confidentiality of fingerprint information. Overall, this PUF system provides a pervasive, flexible multi-level encryption strategy poised for application in print security and beyond. Its combination of concealability, reliability, and adaptability positions it as a promising solution for addressing contemporary security challenges.

4 Experimental section

4.1 Synthesis of dual-color center diamonds

The nano-diamonds (~ 50 nm) were dispersed in ethanol and sonicated for 10 min to obtain a well-dispersed nano-diamond suspension for diamond growth. A germanium metal about 1 micron thick was thermally evaporated on a thin molybdenum sheet for the substrate for diamond growth. Then, the nano-diamond suspension was spin-coated onto the treated substrate as CVD seeds. Si wafers were placed around the substrate to act as a source of silicon doping. Dual-color center micro-diamonds were prepared by MPCVD using H_2 and CH_4 as carrier gas and carbon source, respectively. The $CH_4/(H_2 + CH_4)$ gas ratio was 1%–9%. To prevent germanium melting, the diamond deposition temperature was set at 850 °C during the deposition process for 3–20 h. The resulting sample film was ground in agate mortar for 1 h, and then soaked in hydrofluoric acid overnight to remove silicon impurities. Subsequently, the diamond powder was treated in aqua regia at

260 °C for 12 h, and then washed three times with deionized water to obtain irregular microdiamonds.

4.2 Preparation and use of PUF ink

Initially, AMC purchased from Aladdin Co. Ltd., was dissolved in an alcoholic solution (0.05 g/mL) as an invisible fluorescent agent. Simultaneously, dual-color center diamonds were dispersed into deionized water to achieve a 10 wt.% diamond suspension. Subsequently, equal proportions of the above two solutions were mixed to obtain PUF ink. The dual-color center diamond-based ink was written, sprayed, or sealed onto the target object to form D-PUFs. Long-standing PUF ink required thorough shaking before use.

4.3 Characterization

The crystal structure of dual-color center diamonds was analyzed by XRD patterns (X'Pert Pro, PANalytical, Netherlands). The size distribution of dual-color center diamond was characterized by a scanning electron microscope (JSM-IT200, JEOL, Japan). The surface groups of dual-color center diamonds were determined by FTIR spectroscopy (Nicolet iS10, Thermo Scientific, USA). Raman measurement and photoluminescence (PL) spectroscopy were performed using a spectrometer of the SOL instrument (Confotec MR520, SOL Instruments LTD., Republic of Belarus) equipped with a 532 nm laser with an output power of 50 mW as excitation source and a 20× objective. PL decay curves at 602 and 738 nm were collected using a fluorescence spectrometer (FLS1000, Edinburgh, UK) with a 532 nm picosecond laser.

4.4 Readout and authentication of D-PUFs

The readout of D-PUFs was performed by measuring the broad-spectrum PL of the dual-color center diamond pixel by pixel, with an acquisition time of 0.1 s per pixel, and a 550 nm long-pass filter to filter out stray light. The total readout time of the PUF tag was directly determined by the bit size of the key. By tuning the travelling step of the laser spot, PL mappings with different resolutions (50 × 50 and 100 × 100 pixels) can be acquired in a square area of 200 μm × 200 μm. Each measurement was repeated 3 times, and the position was calibrated before starting. The response matrices based on the distinct response signals can be obtained by further segmenting the integration region of the captured broad-spectrum PL spectra according to the response signals corresponding to the diamond Raman, GeV zero-phonon line, and SiV zero-phonon line, respectively. Subsequently, the developed MATLAB program was employed to extract and analyze the digital keys from the obtained response matrices to complete the digitization and authentication of the multi-level D-PUFs. Ideally, the number of each coding element in the coding matrix should be the same, thus ensuring maximum randomness and encoding capacity. Therefore, we have tailored an encoding strategy that allows for arbitrary-ary encoding, the steps of which are as follows: Initially, the raw PL response matrices were normalized by quantifying the intensity of the PL signal at each pixel; next, a series of non-fixed thresholds (one in binary, nine in decimal and fifteen in hexadecimal) were set to encode the matrices according to the intensity of the response signal from each pixel. For threshold selection, the raw data was sorted according to the magnitude of the values and evenly distributed into M subsets, where M is the number of code elements, and then the maximum value in each subset is extracted as the threshold; then, each pixel was assigned a value based on the thresholds to obtain M-ary keys. Wherein, the binary encoding can directly select the median value as the threshold value; finally, PUF authentication was accomplished by comparing and calculating the differences between two data matrices. Binary coding matrices were authenticated by calculating the Hamming distance. The bit uniformity can be calculated using the following equation

$$\text{Bit unifomity} = \frac{1}{k}\sum_{i=1}^{k} K_i \tag{1}$$

where K_i is the i^{th} binary bit in the PUF digitized keys and k is the key size.

The device uniqueness between any two PUF patterns can be defined as

$$\text{Device uniqueness} = \frac{2}{q(q-1)}\sum_{i=1}^{q-1}\sum_{j=i+1}^{q}\frac{\text{HD}(K_i,K_j)}{t} \tag{2}$$

where K_n and K_m are t-bit keys of the n^{th} PUF device and the m^{th} PUF device, respectively, and q is the total number of PUF labels.

The readout reproducibility can be calculated as the following equation

$$\text{Readout reproducibility} = \sum_{i=1}^{t}\frac{\text{HD}(K_i,K_i')}{t} \tag{3}$$

where K_i is the original t-bit reference binary coding matrix and K_i' is a t-bit binary coding matrix extracted from repeated measurements of the same PUF label.

The similarity index was calculated as a function

$$\text{Similarity index} = 1 - \frac{\sum_{i=1}^{t}\sqrt{(K_i - K_i')^2}}{t} \times 100\% \tag{4}$$

where K is the original t-bit reference binary coding matrix and K' is a t-bit binary coding matrix extracted from repeated measurements of the same PUF.

Verification of M-ary encoding matrices was achieved by performing a cross-correlation function. The cross-correlation coefficient can be defined as

$$R_{xy} = \frac{\text{cov}(x,y)}{(\text{std}(x) * \text{std}(y))} \tag{5}$$

where cov(x,y) denotes the covariance of x and y, and std(x,y) denotes the standard deviation of x and y.

The entropy of bit distribution was calculated as a function

$$H = -\sum_{i=1}^{n}(p(i) * \log_2(p(i))) \tag{6}$$

where H is the information entropy and $p(i)$ is the probability of each category in the data. For the D-PUFs, the value of n can be 2, 10, and 16. Combining 4 different responses, H can be estimated to be 6.

The encoding capacity can be conventionally defined as c^s, where c is the bit states and s is the key size, representing the total number of codes that can be generated. In this work, the bit states can be 16, the key size is 100 × 100 pixels. Combining the four layers of different anti-counterfeiting modes, the encoding capacity can be calculated as $(16^{100\times100})^4 = 16^{40000} > 10^{48164}$.

DoF were adopted to evaluate the number of independent bit sequences, which is calculated as

$$\text{DoF} = \frac{\mu(1-\mu)}{\sigma^2} \tag{7}$$

where μ is the mean of inter-HDs and σ is the standard deviation of inter-HDs.

Each layer response of D-PUFs shows a corresponding DoF of 816 ($\approx 0.4979 \times (1 - 0.4979)/0.0175^2$), 230 ($\approx 0.4992 \times (1 - 0.4992)/0.033^2$), 1068 ($\approx 0.4996 \times (1 - 0.4996)/0.0153^2$), and 1313 ($\approx 0.4993 \times (1 - 0.4993)/0.0138^2$), resulting in an actual encoding capacity of 2^{816}, 2^{230}, 2^{1068} and 2^{1313}, respectively.

4.5 Reliability test

The thermal reliability of the D-PUFs was performed using a heating/cooling stage (T96-S, LINKAM, UK) with temperatures ranging from room temperature to 100 °C at a heating rate of 5 °C/min. For relative humidity (RH) stability, the D-PUFs were placed in airtight glass containers at room temperature (25 °C) for 3 h. Different saturated salt solutions of $CaCl_2$, NH_4Cl, and Na_2CO_3 were used to provide humidity environments, with RHs of 31%, 79%, and 92%, respectively.

Electronic Supplementary Material: Supplementary material (additional material characterization, optical photographs, stability measurements, and M-ary encryption authentication) is available in the online version of this article at https://doi.org/10.26599/NR.2025.94907905.

Data availability

All data needed to support the conclusions in the paper are presented in the manuscript and the Electronic Supplementary Material. Additional data related to this paper may be requested from the corresponding author upon request.

Acknowledgements

The authors thank for the support of the National Key Research and Development Program of China (No. 2022YFB3608604), the National Natural Science Foundation of China (Nos. U22A2077 and U21A2070), Shandong Provincial Natural Science Foundation (No. ZR2022MH280), Medical Science and Technology Project of Shandong Province (No. 202307020692), Natural Science Foundation of Henan (Nos. 212300410020 and 222300420297), Science and Technology Major Project of Henan Province (No. 221100230300), the Fundamental Research Fund of Henan Academy of Sciences (No. 20250627005), and Henan Postdoctoral Foundation (No. 202101007).

Declaration of competing interest

All the contributing authors report no conflict of interests in this work.

Author contribution statement

F. H. J.: Conceptualization, methodology, investigation, data analysis, writing – original draft. J. L. S.: Conceptualization, methodology, investigation, data analysis, writing – original draft. C. N. L.: Methodology, data analysis, writing – original draft, funding acquisition. Z. F. Z.: Resources, investigation. Y. D.: Resources, investigation. H. Z. G.: Validation, writing – review & editing. S. F. L.: Validation, writing – review & editing. L. J. W.: Validation, writing – review & editing. C.-X. S.: Conceptualization, validation, writing – review & editing, supervision, funding acquisition. L. D.: Conceptualization, validation, writing – review & editing, supervision, funding acquisition.

Use of AI statement

None.

References

[1] Park, S. M.; Park, G.; Yoon, D. K. Paintable physical unclonable functions using DNA. *Adv. Mater.* **2023**, *35*, 2302135.

[2] Arppe, R.; Sørensen, T. J. Physical unclonable functions generated through chemical methods for anti-counterfeiting. *Nat. Rev. Chem.* **2017**, *1*, 0031.

[3] Huang, S.; Wu, J. K. Optical watermarking for printed document authentication. *IEEE Trans. Inf. Forensics Secur.* **2007**, *2*, 164–173.

[4] Kang, H.; Stoykova, E.; Kim, Y.; Hong, S.; Park, J.; Hong, J. Color holographic wavefront printing technique for realistic representation. *IEEE Trans. Industr. Inform.* **2016**, *12*, 1590–1598.

[5] Ding, L. J.; Wang, X. D. Luminescent oxygen-sensitive ink to produce highly secured anticounterfeiting labels by inkjet printing. *J. Am. Chem. Soc.* **2020**, *142*, 13558–13564.

[6] Shen, C. L.; Lou, Q.; Lv, C. F.; Zang, J. H.; Qu, S. N.; Dong, L.; Shan, C. X. Bright and multicolor chemiluminescent carbon nanodots for advanced information encryption. *Adv. Sci.* **2019**, *6*, 1802331.

[7] Mao, X.; Liu, K. K.; Cao, Q.; Song, S. Y.; Liang, Y. C.; Hu, Y. W.; Chang, S. L.; Liao, J.; Shan, C. X. Paper-fiber-activated triplet excitons of carbon nanodots for time-resolved anti-counterfeiting signature with artificial intelligence authentication. *ACS Appl. Mater. Interfaces* **2023**, *15*, 20302–20309.

[8] Zhou, X.; Fang, C. Q.; Li, Y.; An, N. L.; Lei, W. Q. Preparation and characterization of Fe_3O_4-CNTs magnetic nanocomposites for potential application in functional magnetic printing ink. *Compos. Part B: Eng.* **2016**, *89*, 295–302.

[9] Dodda, A.; Subbulakshmi Radhakrishnan, S.; Schranghamer, T. F.; Buzzell, D.; Sengupta, P.; Das, S. Graphene-based physically unclonable functions that are reconfigurable and resilient to machine learning attacks. *Nat. Electron.* **2021**, *4*, 364–374.

[10] Zhong, D. L.; Liu, J. X.; Xiao, M. M.; Xie, Y. N.; Shi, H. W.; Liu, L. J.; Zhao, C. Y.; Ding, L.; Peng, L. M.; Zhang, Z. Y. Twin physically unclonable functions based on aligned carbon nanotube arrays. *Nat. Electron.* **2022**, *5*, 424–432.

[11] Gao, Y. S.; Al-Sarawi, S. F.; Abbott, D. Physical unclonable functions. *Nat. Electron.* **2020**, *3*, 81–91.

[12] Gu, Y. Q.; He, C.; Zhang, Y. Q.; Lin, L.; Thackray, B. D.; Ye, J. Gap-enhanced Raman tags for physically unclonable anticounterfeiting labels. *Nat. Commun.* **2020**, *11*, 516.

[13] Carro-Temboury, M. R.; Arppe, R.; Vosch, T.; Sørensen, T. J. An optical authentication system based on imaging of excitation-selected lanthanide luminescence. *Sci. Adv.* **2018**, *4*, e1701384.

[14] Liu, Y.; Han, F.; Li, F. S.; Zhao, Y.; Chen, M. S.; Xu, Z. W.; Zheng, X.; Hu, H. L.; Yao, J. M.; Guo, T. L. et al. Inkjet-printed unclonable quantum dot fluorescent anti-counterfeiting labels with artificial intelligence authentication. *Nat. Commun.* **2019**, *10*, 2409.

[15] Chen, P.; Li, D. Y.; Li, Z. X.; Xu, X.; Wang, H. Y.; Zhou, X.; Zhai, T. Y. Programmable physical unclonable functions using randomly anisotropic two-dimensional flakes. *ACS Nano* **2023**, *17*, 23989–23997.

[16] Kim, M. S.; Lee, G. J.; Leem, J. W.; Choi, S.; Kim, Y. L.; Song, Y. M. Revisiting silk: A lens-free optical physical unclonable function. *Nat. Commun.* **2022**, *13*, 247.

[17] Kim, Y.; Lim, J.; Lim, J. H.; Hwang, E.; Lee, H.; Kim, M.; Ha, I.; Cho, H.; Kwon, J.; Oh, J. et al. Reconfigurable multilevel optical PUF by spatiotemporally programmed crystallization of supersaturated solution. *Adv. Mater.* **2023**, *35*, 2212294.

[18] Sun, N. F.; Chen, Z. Y.; Wang, Y. K.; Wang, S.; Xie, Y.; Liu, Q. Random fractal-enabled physical unclonable functions with dynamic AI authentication. *Nat. Commun.* **2023**, *14*, 2185.
[19] Kim, K.; Kim, S. U.; Choi, M. Y.; Saeed, M. H.; Kim, Y.; Na, J. H. Voxelated opto-physically unclonable functions via irreplicable wrinkles. *Light: Sci. Appl.* **2023**, *12*, 245.
[20] Martinez, P.; Papagiannouli, I.; Descamps, D.; Petit, S.; Marthelot, J.; Lévy, A.; Fabre, B.; Dory, J. B.; Bernier, N.; Raty, J. Y. et al. Laser generation of sub-micrometer wrinkles in a chalcogenide glass film as physical unclonable functions. *Adv. Mater.* **2020**, *32*, 2003032.
[21] Park, G.; Park, H.; Wolska, J. M.; Park, J. G.; Yoon, D. K. Racemized photonic crystals for physical unclonable function. *Mater. Horiz.* **2022**, *9*, 2542–2550.
[22] Jing, L.; Xie, Q.; Li, H. L.; Li, K. R.; Yang, H. T.; Ng, P. L. P.; Li, S.; Li, Y.; Teo, E. H. T.; Wang, X. N. et al. Multigenerational crumpling of 2D materials for anticounterfeiting patterns with deep learning authentication. *Matter* **2020**, *3*, 2160–2180.
[23] Minh, D. N.; Nguyen, L. A. T.; Nguyen, Q. H.; Van Vu, T.; Choi, J.; Eom, S.; Kwon, S. J.; Kang, Y. Synthesis of $MAPbBr_3$-polymer composite films by photolysis of DMF: Toward transparent and flexible optical physical unclonable functions (PUFs) with hierarchical multilevel complexity. *Adv. Mater.* **2023**, *35*, 2208151.
[24] Sun, H.; Maji, S.; Chandrakasan, A. P.; Marelli, B. Integrating biopolymer design with physical unclonable functions for anticounterfeiting and product traceability in agriculture. *Sci. Adv.* **2023**, *9*, eadf1978.
[25] Kim, J. H.; Jeon, S.; In, J. H.; Nam, S.; Jin, H. M.; Han, K. H.; Yang, G. G.; Choi, H. J.; Kim, K. M.; Shin, J. et al. Nanoscale physical unclonable function labels based on block copolymer self-assembly. *Nat. Electron.* **2022**, *5*, 433–442.
[26] Wang, J. Y.; Zhang, Q.; Chen, R. Z.; Li, J.; Wang, J. H.; Hu, G. Y.; Cui, M. Y.; Jiang, X.; Song, B.; He, Y. Triple-layer unclonable anti-counterfeiting enabled by huge-encoding capacity algorithm and artificial intelligence authentication. *Nano Today* **2021**, *41*, 101324.
[27] Daqiqeh Rezaei, S.; Dong, Z. G.; Wang, H.; Xu, J. H.; Wang, H. T.; Tavakkoli Yaraki, M.; Choon Hwa Goh, K.; Zhang, W.; Ghorbani, S. R.; Liu, X. G. et al. Tri-functional metasurface enhanced with a physically unclonable function. *Mater. Today* **2023**, *62*, 51–61.
[28] Lapidas, V.; Zhizhchenko, A.; Pustovalov, E.; Storozhenko, D.; Kuchmizhak, A. Direct laser printing of high-resolution physically unclonable function anti-counterfeit labels. *Appl. Phys. Lett.* **2022**, *120*, 261104.
[29] Miller, B. S.; Bezinge, L.; Gliddon, H. D.; Huang, D.; Dold, G.; Gray, E. R.; Heaney, J.; Dobson, P. J.; Nastouli, E.; Morton, J. J. L. et al. Spin-enhanced nanodiamond biosensing for ultrasensitive diagnostics. *Nature* **2020**, *587*, 588–593.
[30] Rovny, J.; Yuan, Z. Y.; Fitzpatrick, M.; Abdalla, A. I.; Futamura, L.; Fox, C.; Cambria, M. C.; Kolkowitz, S.; de Leon, N. P. Nanoscale covariance magnetometry with diamond quantum sensors. *Science* **2022**, *378*, 1301–1305.
[31] Zhang, T. T.; Wang, L. Z.; Wang, J.; Wang, Z. Q.; Gupta, M.; Guo, X. Y.; Zhu, Y.; Yiu, Y. C.; Hui, T. K. C.; Zhou, Y. et al. Multimodal dynamic and unclonable anti-counterfeiting using robust diamond microparticles on heterogeneous substrate. *Nat. Commun.* **2023**, *14*, 2507.
[32] Hu, Y. W.; Zhang, T. P.; Wang, C. F.; Liu, K. K.; Sun, Y.; Li, L.; Lv, C. F.; Liang, Y. C.; Jiao, F. H.; Zhao, W. B. et al. Flexible and biocompatible physical unclonable function anti-counterfeiting label. *Adv. Funct. Mater.* **2021**, *31*, 2102108.
[33] Wang, L. Z.; Yu, X.; Zhang, T. T.; Hou, Y.; Lei, D. Y.; Qi, X. J.; Chu, Z. Q. High-dimensional anticounterfeiting nanodiamonds authenticated with deep metric learning. *Nat. Commun.* **2024**, *15*, 10602.
[34] Guo, H.; Qin, Y.; Wang, Z. B.; Ma, Y. X.; Wen, H. F.; Li, Z. H.; Ma, Z. M.; Li, X.; Tang, J.; Liu, J. Multilevel encoding physically unclonable functions based on the multispecies structure in diamonds. *Adv. Funct. Mater.* **2024**, *34*, 2304648.
[35] Jiao, F. H.; Lin, C. N.; Dong, L.; Mao, X.; Wu, Y.; Dong, F. Y.; Zhang, Z. F.; Sun, J. L.; Li, S. F.; Yang, X. et al. Silicon vacancies diamond/silk/PVA hierarchical physical unclonable functions for multi-level encryption. *Adv. Sci.* **2024**, *11*, 2308337.
[36] Jiao, F. H.; Lin, C. N.; Dong, L.; Wu, Y.; Xiao, Y.; Zhang, Z. F.; Sun, J. L.; Zhao, W. B.; Li, S. F.; Yang, X. et al. Traceable optical physical unclonable functions based on germanium vacancy in diamonds. *ACS Appl. Mater. Interfaces* **2024**, *16*, 44328–44339.
[37] Bradac, C.; Gao, W. B.; Forneris, J.; Trusheim, M. E.; Aharonovich, I. Quantum nanophotonics with group IV defects in diamond. *Nat. Commun.* **2019**, *10*, 5625.
[38] Westerhausen, M. T.; Trycz, A. T.; Stewart, C.; Nonahal, M.; Regan, B.; Kianinia, M.; Aharonovich, I. Controlled doping of GeV and SnV color centers in diamond using chemical vapor deposition. *ACS Appl. Mater. Interfaces* **2020**, *12*, 29700–29705.
[39] Liu, Y.; Zheng, Y. H.; Zhu, Y. B.; Ma, F. M.; Zheng, X. J.; Yang, K. Y.; Zheng, X.; Xu, Z. W.; Ju, S. M.; Zheng, Y. T. et al. Unclonable perovskite fluorescent dots with fingerprint pattern for multilevel anticounterfeiting. *ACS Appl. Mater. Interfaces* **2020**, *12*, 39649–39656.
[40] Zhang, J. F.; Creamer, A.; Xie, K.; Tang, J. Q.; Salter, L.; Wojciechowski, J. P.; Stevens, M. M. Bright and stable anti-counterfeiting devices with independent stochastic processes covering multiple length scales. *Nat. Commun.* **2025**, *16*, 502.
[41] Lai, S. L.; Shen, W. X.; Zhang, Z. F.; Fang, C.; Zhang, Y. W.; Chen, L. C.; Wang, Q. Q.; Wan, B.; Jia, X. P. High-pressure high-temperature industrial preparation of micron-sized diamond single crystals with silicon-vacancy colour centres. *Int. J. Refract. Met. Hard Mater.* **2022**, *105*, 105806.
[42] Wang, M. Q.; Sun, H. Y.; Ye, X. Y.; Yu, P.; Liu, H. Y.; Zhou, J. W.; Wang, P. F.; Shi, F. Z.; Wang, Y.; Du, J. F. Self-aligned patterning technique for fabricating high-performance diamond sensor arrays with nanoscale precision. *Sci. Adv.* **2022**, *8*, eabn9573.
[43] Zhang, Z. F.; Lin, C. N.; Yang, X.; Tian, Y. Z.; Gao, C. J.; Li, K. Y.; Zang, J. H.; Yang, X. G.; Dong, L.; Shan, C. X. Solar-blind imaging based on 2-inch polycrystalline diamond photodetector linear array. *Carbon* **2021**, *173*, 427–432.
[44] Li, C. X.; Zhang, X.; Oliveira, E. F.; Puthirath, A. B.; Neupane, M. R.; Weil, J. D.; Birdwell, A. G.; Ivanov, T. G.; Kong, S.; Gray, T. et al. Systematic comparison of various oxidation treatments on diamond surface. *Carbon* **2021**, *182*, 725–734.
[45] Li, F. K.; Zhao, W. B.; Wang, Y.; Huang, W. T.; Ku, Y. L.; Liu, H.; Guo, R.; Yu, H. H.; Liu, K. K.; Shan, C. X. Cationic engineered nanodiamonds for efficient antibacterial surface with strong wear resistance. *Nano Res.* **2024**, *17*, 939–948.
[46] Liu, X. Z.; Wang, Y. Q.; Wang, G. Y.; Ma, Y. F.; Zheng, Z. H.; Fan, K. K.; Liu, J. C.; Zhou, B. Q.; Wang, G.; You, Z. et al. An ultrasound-driven implantable wireless energy harvesting system using a triboelectric transducer. *Matter* **2022**, *5*, 4315–4331.
[47] Jiao, F. H.; Zhao, W.; Zhao, W. B.; Wang, Y.; Deng, Y.; Chang, S. L.; Sun, J. L.; Lou, Q.; Wang, L. J.; Shan, C. X. et al. Biomass-derived washable composites for accelerating the healing of infected wounds. *BMEMat* **2023**, *1*, e12055.